Monthly Notices
of the
ROYAL ASTRONOMICAL SOCIETY

MNRAS **433,** 825–837 (2013)
Advance Access publication 2013 June 4

doi:10.1093/mnras/stt777

The importance of major mergers in the build up of stellar mass in brightest cluster galaxies at $z = 1$

C. Lidman,[1⋆] G. Iacobuta,[1,2] A. E. Bauer,[1] L. F. Barrientos,[3] P. Cerulo,[4] W. J. Couch,[4] L. Delaye,[5] R. Demarco,[6] E. Ellingson,[7] A. J. Faloon,[8] D. Gilbank,[9] M. Huertas-Company,[5,10] S. Mei,[5,10] J. Meyers,[11] A. Muzzin,[12] A. Noble,[8] J. Nantais,[6] A. Rettura,[13] P. Rosati,[14] R. Sánchez-Janssen,[15] V. Strazzullo,[16] T. M. A. Webb,[8] G. Wilson,[17] R. Yan[18] and H. K. C. Yee[19]

[1]*Australian Astronomical Observatory, PO Box 915, North Ryde, NSW 1670, Australia*
[2]*School of Physics and Astronomy, University of Nottingham, University Park, Nottingham NG7 2RD, UK*
[3]*Departamento de Astronomía y Astrofísica Pontifica Universidad Cathólica de Chile, Vicuña MacKenna 4860, Casilla 386, Santiago 22, Chile*
[4]*Centre for Astrophysics and Supercomputing, Swinburne University of Technology, PO Box 218, Hawthorn, VIC 3122, Australia*
[5]*GEPI, Observatoire de Paris, 77 Avenue Denfert-Rochereau, F-70514 Paris, France*
[6]*Department of Astronomy, Universidad de Concepcion, Casilla 160-C Concepcion, Chile*
[7]*Center for Astrophysics and Space Astronomy, Department of Astrophysical and Planetary Science, UCB-389, University of Colorado, Boulder, CO 80309, USA*
[8]*McGill University, 3600 rue University, Montreal, QC H3A 2T8, Canada*
[9]*South African Astronomical Observatory, PO Box 9, Observatory, 7935, South Africa*
[10]*Université Paris Denis Diderot, F-75205 Paris Cedex 13, France*
[11]*Department of Physics, Stanford University, 450 Serra Mall Stanford, CA 94305, USA*
[12]*Leiden Observatory, Leiden University, PO Box 9513, 2300 RA Leiden, the Netherlands*
[13]*Jet Propulsion Laboratory, 4800 Oak Grove Drive, Pasadena, CA 91109, USA*
[14]*European Southern Observatory, Karl-Schwarzschild Strasse 2, D-85748 Garching, Germany*
[15]*European Southern Observatory, Alonso de Cordova 3107, Vitacura, Casilla 19001, Santiago 19, Chile*
[16]*Laboratoire AIM-Paris-Saclay, CEA/DSM-CNRS, Universit Paris Diderot, Irfu/Service d'Astrophysique, CEA Saclay, Orme des Merisiers, F-91191 Gif sur Yvette, France*
[17]*Department of Physics and Astronomy, University of California, Riverside, CA 92521, USA*
[18]*Department of Physics and Astronomy, University of Kentucky, 505 Rose St Lexington, KY 40506-0055, USA*
[19]*Department of Astronomy and Physics, University of Toronto, Toronto, Ontario M5S 3H4, Canada*

Accepted 2013 May 1. Received 2013 April 18; in original form 2013 March 7

ABSTRACT

Recent independent results from numerical simulations and observations have shown that brightest cluster galaxies (BCGs) have increased their stellar mass by a factor of almost 2 between $z \sim 0.9$ and $z \sim 0.2$. The numerical simulations further suggest that more than half this mass is accreted through major mergers. Using a sample of 18 distant galaxy clusters with over 600 spectroscopically confirmed cluster members between them, we search for observational evidence that major mergers do play a significant role. We find a major merger rate of 0.38 ± 0.14 mergers per Gyr at $z \sim 1$. While the uncertainties, which stem from the small size of our sample, are relatively large, our rate is consistent with the results that are derived from numerical simulations. If we assume that this rate continues to the present day and that half of the mass of the companion is accreted on to the BCG during these mergers, then we find that this rate can explain the growth in the stellar mass of the BCGs that is observed and predicted by simulations. Major mergers therefore appear to be playing an important role, perhaps even the dominant one, in the build up of stellar mass in these extraordinary galaxies.

Key words: galaxies: clusters: general – galaxies: evolution – galaxies: high-redshift.

1 INTRODUCTION

Brightest cluster galaxies (BCGs) are amongst the largest, most massive and most luminous galaxies in the Universe. Often found

⋆E-mail: clidman@aao.gov.au

close to the centre of the cluster that they inhabit, BCGs are generally easy to identify, even in the most distant clusters that are currently known. They are also easy to identify in large *N*-body simulations, thus allowing us the opportunity to directly compare, for a single class of galaxy, the predictions of numerical simulations with observations.

In the hierarchical scenario for the formation of structure in our universe, BCGs build up their stellar mass over time by converting material accreted from their surroundings into stars and by merging with other galaxies. Over the range of redshifts that we can observe BCGs, the stellar mass of the average BCG is expected to increase significantly with time through merging with other galaxies. For example, in the semi-analytic model described in De Lucia & Blaizot (2007), the stellar mass increases by a factor of 4 between redshift $z = 1.0$ and today.

Observationally, it appears that the growth is slightly slower than the predictions of the De Lucia & Blaizot (2007) model. From a sample of 150 BCGs, Lidman et al. (2012) found that the stellar mass of BCGs increases by a factor of 1.8 over the redshift interval $z \sim 0.9-0.2$. This result differs from that of earlier works, which generally found little or no change over the same redshift interval (Stott et al. 2008; Whiley et al. 2008; Collins et al. 2009; Stott et al. 2010). In part, this was due to the way the positive correlation between the mass of the cluster and the stellar mass of the BCG (Edge 1991; Burke, Collins & Mann 2000; Brough et al. 2002, 2008; Stott et al. 2008) tends to dilute the observed evolution. The distant clusters used in these samples were more massive than the likely progenitors of clusters in the low-redshift comparison samples. The distant clusters therefore tended to have more massive BCGs to start with.

More recent models (Laporte et al. 2013) predict that BCGs should increase their stellar mass by a factor of 1.9 between $z = 1.0$ and $z = 0.2$, an increase that is lower than that reported in earlier simulations (De Lucia & Blaizot 2007). The theoretical expectation and the observations are now in excellent agreement. The new models also predict that the growth occurs through a combination of minor and major mergers[1] and that the size of BCGs should increase dramatically as they grow in mass.

Observational support for the notion that BCGs build up their stellar mass by merging has been steadily increasing over the past few years. From a sample of 91 BCGs at $z \sim 0.3$, Edwards & Patton (2012) found that BCGs increase their mass by as much as 10 per cent over 0.5 Gyr. Both minor and major mergers are thought to play a role, with major mergers contributing somewhere between half (Edwards & Patton 2012) to substantially more than half (Hopkins et al. 2010; Laporte et al. 2013) of the mass. Direct evidence for merging, through tidal tails and distorted isophotes, has been found by a number of authors (McIntosh et al. 2008; Liu et al. 2009; Rasmussen et al. 2010; Brough et al. 2011; Bildfell et al. 2013). Liu et al. (2009) estimated that 3.5 per cent of BCGs in the redshift interval $0.03 \leq z \leq 0.12$ show evidence for an ongoing merger. McIntosh et al. (2008) found a similar fraction and estimated that the centres of groups and clusters are increasing their mass at a rate of 2–9 per cent per Gyr. Once signs of a merger are evident, the time-scale for merging is short, of the order of a few crossing times, which is typically around 0.2 Gyr for galaxies that are within 30 kpc of the BCG.

[1] Throughout this paper we use $0.25 < \mu_\star < 1$ to define a major merger, where $\mu_\star$ is the mass ratio between the satellite and its more massive companion.

The amount of mass accreted through mergers by BCGs in distant clusters, i.e. those at $z \sim 1$, is largely unconstrained. A measurement of the mass accreted by high-redshift BCGs can be combined with the measurements at low redshift, and allow us to estimate the mass accreted through mergers from redshift 1 to today.

In this paper, we combine high-quality ground-based near-IR images of a sample of 18 distant galaxy clusters with extensive spectroscopy to examine the possibility that major mergers between the brightest galaxies within the core of the cluster and the BCG contribute significantly to the growth of the stellar mass of the BCG between $z \sim 1$ and today. In Section 2, we introduce the sample that we use in the analysis, which includes new high-resolution data taken with the HAWK-I[2] camera on the Very Large Telescope (VLT). Since much of the HAWK-I data have not been published before and since we will make these data public, we provide a detailed description of how these data were taken and processed. After expanding the work presented in Lidman et al. (2012) by adding new measurements to the rest-frame *K*-band magnitude–redshift relation in Section 3, we use the radial distribution of over 600 spectroscopically confirmed cluster galaxies, both bright and faint, to argue in Section 4 that there is an excess of bright galaxies close to the BCG. We then estimate the time-scale for the brighter galaxies to merge with the BCG and then infer how many close companions we should have seen if major merging is the dominant process for the build-up of stellar mass in BCGs. In the final two sections of the paper, we discuss and summarize our main results.

Throughout the paper, all magnitudes and colours are measured in the observer frame and are placed on the 2MASS photometric system. Vega magnitudes are used throughout. We also assume a flat cold dark matter cosmology with $\Omega_\Lambda = 0.73$ and $H_0 = 70\,\mathrm{km\,s^{-1}\,Mpc^{-1}}$.

2 THE CLUSTER SAMPLE

The sample of clusters we use in this paper is built from several surveys. 10 clusters come from SpARCS[3] (Muzzin et al. 2009; Wilson et al. 2009). In brief, the SpARCS clusters were discovered by searching for overdensities in the number of red galaxies using images taken with IRAC on the *Spitzer Space Telescope* and ground-based *z*-band images taken with either MegaCam on the Canada–France–Hawaii Telescope or MOSAIC II on the Cerro Tololo Blanco Telescope. Additional details on individual clusters can be found in Muzzin et al. (2009), Wilson et al. (2009) and Demarco et al. (2010a).

All 10 clusters from SpARCS were also part of GCLASS,[4] a spectroscopic survey that used the multi-object spectroscopic (MOS) modes of GMOS-N and GMOS-S on the Gemini Telescopes to obtain between 20 and 80 spectroscopically confirmed members per cluster (Muzzin et al. 2012). The comprehensive spectroscopic coverage provided by GCLASS allows us to identify the brightest cluster members in each of the clusters, and to exclude foreground and background galaxies that might be confused as cluster members. It is for this reason that we do not add the two SpARCS clusters at $z \sim 1.63$ in Lidman et al. (2012) to the sample. The number of spectroscopically confirmed cluster members is currently around

[2] High Acuity Wide field K-band Imager.

[3] Spitzer Adaptation of the Red-Sequence Cluster Survey, www.faculty.ucr.edu/∼gillianw/SpARCS/.

[4] Gemini Cluster Astrophysics Spectroscopic Survey, www.faculty.ucr.edu/∼gillianw/GCLASS/.

Table 1. The 19 clusters in our initial sample. Listed first are clusters from the HCS, followed by clusters from SpARCS.

Name	Abbreviated name	Redshift	Discovery method	Members[a]	References
RX J0152.7−1357	RX 0152	0.8360	X-ray	109	Demarco et al. (2005)
RCS 231953+0038.0	RCS 2319	0.9024	Optical	25	Gilbank et al. (2008)
XMMU J1229.4+0151	XMMU 1229	0.9755	X-ray	18	Santos et al. (2009)
RCS 022056−0333.4	RCS 0220	1.0271	Optical	7	Muñoz (2009)
RCS 234526−3632.6	RCS 2345	1.0360	Optical	29	Muñoz (2009)
XLSS J0223.0−0436	XLSS 0233	1.2132	X-ray/Optical–IR	20	Bremer et al. (2006)
RDCS J1252.9−2927	RDCS 1252	1.2380	X-ray	42	Rosati et al. (2004)
XMMU J2235.3−2557	XMMU 2235	1.3900	X-ray	25	Mullis et al. (2005)
XMMXCS J2215.9−1738	XMMXCS 2215	1.4600	X-ray	26	Stanford et al. (2006)
SpARCS J003442−430752	SpARCS 0034	0.867	Optical–IR	39	Muzzin et al. (2012)
SpARCS J003645−441050	SpARCS 0036	0.869	Optical–IR	46	Muzzin et al. (2012)
SpARCS J161314+564930	SpARCS 1613	0.871	Optical–IR	87	Demarco et al. (2010a)
SpARCS J104737+574137	SpARCS 1047	0.956	Optical–IR	26	Muzzin et al. (2012)
SpARCS J021524−034331	SpARCS 0215	1.004	Optical–IR	42	Muzzin et al. (2012)
SpARCS J105111+581803	SpARCS 1051	1.035	Optical–IR	26	Muzzin et al. (2012)
SpARCS J161641+554513	SpARCS 1616	1.156	Optical–IR	37	Demarco et al. (2010a)
SpARCS J163435+402151	SpARCS 1634	1.177	Optical–IR	35	Muzzin et al. (2009)
SpARCS J163852+403843	SpARCS 1638	1.195	Optical–IR	18	Muzzin et al. (2009)
SpARCS J003550−431224	SpARCS 0035	1.335	Optical–IR	21	Wilson et al. (2009)

[a]The number of spectroscopically confirmed members within r_{200} of the cluster centre and with peculiar velocities that are less than three times the cluster velocity dispersion. r_{200} is the radius within which the mean density of the cluster equals the critical density of the Universe at the redshift of the cluster multiplied by a factor of 200.

a dozen for both clusters, although work to increase this number significantly is currently underway.

Complementing the comprehensive spectroscopic coverage are ground-based images in the optical (*u, g, r, i* and *z*) and near-IR (*J* and K_s), images in each of the IRAC passbands ([3.6], [4.5], [5.8] and [8]), and for some clusters, images with MIPS on the Spitzer Space Telescope. The near-IR data are described in Lidman et al. (2012), while the optical data are described in van der Berg et al. (2013).

The remaining clusters were discovered either through their X-ray emission or as overdensities of red galaxies. Most of these clusters were observed with HAWK-I as part of the HAWK-I cluster survey, which we describe in greater detail in the following section. All clusters are listed in Table 1. The redshift range covered by the sample extends from $z = 0.84$ to $z = 1.46$.

2.1 The HAWK-I cluster survey

During 2005 and 2006, the Supernova Cosmology Project targeted 25 galaxy clusters in the redshift range $0.9 < z < 1.5$ with the ACS camera on *Hubble Space Telescope* (*HST*) with the purpose of finding distant Type Ia supernovae (SNe Ia). The survey was called the *HST* Cluster Supernova Survey, and is described in Dawson et al. (2009). Given the relatively small fields of view that are available with *HST* and the high surface density of potential hosts in distant clusters, distant clusters are an efficient way of finding distant SNe Ia (Dawson et al. 2009; Suzuki et al. 2012).

Clusters for the *HST* Cluster Supernova Survey were selected from the IRAC Shallow Cluster Survey (Eisenhardt et al. 2008), the Red-sequence Cluster Surveys (RCS and RCS-2; Gladders & Yee 2005; Yee et al. 2007), the XMM Cluster Survey (Sahlén et al. 2009), the Palomar Distant Cluster Survey (Postman et al. 1996), the *XMM–Newton* Distant Cluster Project (Boehringer et al. 2005) and the *ROSAT* Deep Cluster Survey (RDCS; Rosati et al. 1999). At the time the *HST* Cluster Supernova Survey was conducted, the sample represented a significant fraction of the known $z > 0.9$ clusters.

The spectroscopic follow-up of supernovae in these clusters was done with FORS2 on the VLT, LRIS on Keck and FOCAS on Subaru. Details on the follow-up can be found in Dawson et al. (2009) and Morokuma et al. (2010). In most cases, the MOS mode was used, which allowed one to obtain the redshifts of many cluster members in addition to that of the host of the supernova or the supernova itself. Some clusters, such as XMMU 1229 (Santos et al. 2009), produced several SNe, which meant that they were targeted multiple times, thereby leading to many redshifts.

Many of the clusters in the *HST* Cluster Supernova Survey have been observed at other wavelengths. This includes longer wavelength data taken with IRAC and MIPS on the *Spitzer Space Telescope* and, for a few clusters, data from the *Herschel Space Observatory*. This broad coverage, together with the large number of spectroscopically confirmed cluster members in each cluster means that these clusters are an ideal sample for studying the properties of galaxies in distant clusters. Lacking, however, were high-quality near-IR data that matched the depth of the data taken in space. This was the driving reason for observing many of these clusters with HAWK-I on the VLT in a survey that we refer to in the rest of the paper as the HAWK-I cluster survey (HCS).

Clusters for the HCS were selected from those targeted in the *HST* Cluster Supernova Survey according to two criteria:

(i) they were visible from the Paranal Observatory,

(ii) there were at least 10 spectroscopically confirmed members per cluster.

To this list, we added RX J0152.7−1357 (hereafter, RX 0152) a X-ray discovered cluster at $z = 0.84$ that has over 100 spectroscopically confirmed cluster members (Demarco et al. 2010b) and deep ACS imaging (Blakeslee et al. 2006).

Six of the nine clusters were discovered from their X-ray emission. One of these, XLSS 0223, was independently discovered as an overdensity of galaxies in images taken with IRAC (Andreon et al. 2005; Bremer et al. 2006; Muzzin et al. 2013). The remainder were discovered as overdensities of red sequence galaxies in the RCS (Gladders & Yee 2005).

Table 2. Observing log.

Name	Instrument	Filter	Exposure time (s)	Image quality (arcsec)	5σ detection limit[a, b] (mag)
RX J0152.7−1357	HAWK-I	K_s	9600	0.35	22.8
RCS 231953+0038.0	HAWK-I	K_s	9600	0.40	22.6
XMMU J1229.4+0151	HAWK-I	K_s	11 310	0.35	23.2
RCS 022056−0333.4	HAWK-I	K_s	9600	0.31	23.1
RCS 234526−3632.6	HAWK-I	K_s	9600	0.35	22.9
XLSS J0223.0−0436	HAWK-I	J	11 040	0.32	24.5
XLSS J0223.0−0436	HAWK-I	K_s	9600	0.32	22.9
RDCS J1252.9−2927	ISAAC	J_s	86 640	0.44	25.1
RDCS J1252.9−2927	ISAAC	K_s	81 990	0.38	23.5
XMMU J2235.3−2557	HAWK-I	J	10 560	0.46	24.0
XMMU J2235.3−2557	HAWK-I	K_s	10 740	0.31	22.5
XMMXCS J2215.9−1738	HAWK-I	J	14 400	0.47	24.1
XMMXCS J2215.9−1738	HAWK-I	K_s	9600	0.35	23.0

[a] All quantities refer to the central part of each image, where the image depth is greatest.
[b] The detection limit is the 5σ point source detection limit within an aperture that has a diameter equal to twice the image quality. It takes into account the correlation in the noise between pixels and does not include the flux that falls outside the aperture.

The complete list of 19 clusters, which includes the clusters from SpARCS, the method by which they were discovered, their redshifts and a list of selected references are listed in Table 1. Also listed are the abbreviated names that we use throughout the text.

2.2 Observations with HAWK-I

Eight of the nine clusters in the HCS were imaged with HAWK-I on Yepun (VLT-UT4) at the ESO Cerro Paranal Observatory. HAWK-I (Pirard et al. 2004; Casali et al. 2006) is a near-IR imager with a 7.5 arcmin × 7.5 arcmin field of view. The focal plane consists of a mosaic of four Hawaii-2RG detectors and results in an average pixel scale of 0.1065 arcsec per pixel. All clusters were imaged in K_s. Clusters above redshift $z = 1.2$ were also imaged in J in order to have two filters, in tandem with z_{850}, closely bracketing the 4000 Å break. At $z \sim 1.2$, the 4000 Å break starts to move out of the ACS z_{850} bandpass.

One other cluster, RDCS 1252,[5] had existing deep ISAAC[6] J and K_s band data. The ISAAC data on RDCS 1252 are exceptionally deep (Lidman et al. 2004), so additional data with HAWK-I were not needed.

In the remainder of this section, we refer to the seven clusters that were observed as part of ESO programme 084.A-0214. This excludes RDCS 1252 and XMMU 2235. The near-IR data on these clusters are fully described in Lidman et al. (2004, 2008).

In order to cover a wide area and to keep the clusters away from the gaps between the detectors, the observations were not done with the cluster positioned in the centre of the mosaic. Instead, a pair of pointings with the cluster roughly centred in quadrants 1 and 3 of the mosaic was used. The two quadrants were chosen as they have the highest quantum efficiency. The resulting union of images covers 10 arcmin by 10 arcmin of the sky.

Individual exposures lasted 20 s in J and 10 s in K_s, and six of these were averaged to form a single image. Between images, the telescope was moved by 10 arcsec to 30 arcsec in a semirandom manner, and 23 (40 for K_s) images were taken in this way in a single observing block. The sequence was repeated several times. Total exposure times, detection limits and other observing details are reported in Table 2.

Zero-points were set using stars from the 2MASS point source catalogue (Skrutskie et al. 2006). Typically, around 10–20 unsaturated 2MASS stars with 2MASS quality flags of 'A' or 'B' were selected to measure zero-points and their uncertainties. 2MASS stars were weighted by the reported uncertainties in the 2MASS point source catalogue. Standard stars from Persson et al. (1998) were observed on some of the nights our fields were observed. The agreement between the zero-points derived from the standards and the zero-points derived using 2MASS stars was always better than 5 per cent and was generally around 2 per cent.

2.3 Data processing

The processing of the raw data was done in a standard manner and largely follows the steps outlined in Lidman et al. (2008). A few minor refinements were made. As in Lidman et al. (2008), SCAMP (version 1.6.2) and SWARP (version 2.17.6)[7] were used to place the images on to a common astrometric reference frame; however, we did not use SWARP to combine images. Instead, we used the IRAF[8] task IMCOMBINE to combine the images processed by SWARP. We weighted the images that went into the combined image with the inverse square of the full width at half-maximum (FWHM) of the point spread function (PSF).

Both the HAWK-I data on XMMU 2235, presented in Lidman et al. (2008), and the ISAAC data on RDCS 1252, presented in Lidman et al. (2004), were reprocessed to match the processing done here.

The quality of data as measured by the image quality in the stacked images and the depth of the images is very high. The image quality (FWHM) is never poorer than 0.5 arcsec and is often better than 0.4 arcsec, while the $5\,\sigma$ detection limits in the K_s-band are 5–6 mag fainter than the BCGs.

[5] We use abbreviated names throughout the paper. The full names are given in Table 1.
[6] ISAAC stands for Infrared Spectrometer and Array Camera.
[7] http://www.astromatic.net/
[8] IRAF is distributed by the National Optical Astronomy Observatories which are operated by the Association of Universities for Research in Astronomy, Inc., under the cooperative agreement with the National Science Foundation.

Table 3. Percentage of galaxies near to the red sequence and within 250 and 500 kpc of the cluster centre with redshifts.

Brightness range[a]	Completeness	
	(250 kpc)	(500 kpc)
1–3	100	85
0.5–1	93	90
0.33–0.5	81	71
0.25–0.33	80	76
0.1–0.25	67	64
0.25–1	85	78

[a]The range is relative to the luminosity of the BCG in the K_s band. For example, 1–3 refers to galaxies that are between one to three times brighter than the BCG.

2.4 Spectroscopic completeness

We noted earlier that there has been extensive spectroscopic follow-up of the clusters in our sample, leading to a large number of objects with redshifts. To estimate the redshift completeness, we first construct colour–magnitude diagrams of all clusters for which we have J and K_s images of comparable quality and depth (13 clusters in total), and then select all galaxies that are within 0.2 mag of the red sequence. We take this galaxy subsample and count the number of galaxies that have redshifts (whether they are cluster members or not) and the number of galaxies that do not have redshifts. We compute these numbers in five bins. The boundaries of the bins correspond to six flux ratios: galaxies that are three times brighter (as measured in the observer-frame K_s band) than the BCG, galaxies that are as bright as the BCG and galaxies that are one-half, one-third, one-quarter and one-tenth as bright as the BCG. We then compute the fraction of galaxies that have redshifts (the spectroscopic completeness) for each of these bins.

The completeness depends on the radius within which one chooses to count galaxies. It reaches an average of about 90 per cent at 250 kpc for objects that brighter than one-quarter of the brightness of the BCG, and then steadily drops with increasing radius. To demonstrate the completeness, we choose two radii: 250 and 500 kpc. The results are displayed in Table 3.

For galaxies that are brighter than the BCG, we are (85) 100 per cent complete within (500) 250 kpc of the cluster centre. The completeness steadily drops as one goes to fainter magnitudes. In the following section, we discuss how the spectroscopic incompleteness may bias the choice of which galaxy is the BCG.

In addition to examining the entire sample, we examined the SpARCS and HCS samples separately, since the spectroscopic follow-up of the HCS and SpARCS clusters differ. The spectroscopic follow-up of the SpARCS clusters involved a single programme (GCLASS) using GMOS-South and GMOS-North at the Gemini Observatory (Muzzin et al. 2012), whereas the follow-up of the HCS clusters involved multiple instruments at multiple observatories and was spread over about 10 years. Broadly speaking, the completeness of the two samples are similar, with GCLASS being slightly more complete in the three faintest bins.

3 BRIGHTEST CLUSTER GALAXIES

3.1 Selecting the BCG

From our initial sample of 19 clusters, we exclude RCS 0220. The central region of RCS 0220 is partially obscured by a nearby, almost face-on spiral galaxy. The spiral galaxy adds an extra degree of uncertainty in identifying the BCG and measuring its flux, because the BCG could be obscured by the spiral. We note that none of our conclusions change if we had chosen to keep this cluster.

From the 18 clusters that remain, we then use the following criteria to select the BCG.

(i) The velocity of the galaxy relative to the systemic velocity of the cluster is less than three times the cluster velocity dispersion.

(ii) The galaxy lies within r_{200} of the luminosity weighted centroid of spectroscopically confirmed cluster members. We compute r_{200} using either X-ray-derived masses, if available, or the measured velocity dispersion, if not.

(iii) The galaxy is the brightest galaxy in the K_s band that remains.

The BCGs of the SpARCS clusters are discussed in Lidman et al. (2012), so here we concentrate on the BCGs in the HCS clusters. The BCGs in the HCS generally lie within 100 kpc of the centres of their respective clusters. There are few notable exceptions, which we discuss here. Thumbnails centred on the BCGs in the HCS clusters are shown in Fig. 1 and coordinates of the BCGs are listed in Table 4.

RX 0152 consists of at least three dynamically distinct clumps (Demarco et al. 2005, 2010b). The two main clumps, which we refer to as the northern and southern clumps, are separated from each other by about 1.5 arcmin (700 kpc). Both clumps emit in the X-ray (Demarco et al. 2005). For this cluster, the BCG is not centred in either of the clumps but centred about 35 arcsec (270 kpc) north-east of the northern clump. It is interesting to note that the brightest galaxies that are centred in these clumps share a common characteristic. Neither one is the BCG of the cluster and both have bright nearby companions. The companion of the galaxy that is centred in the southern clump is only 0.5 arcsec (3.5 kpc) away. These two galaxies were selected as the BCG in Stott et al. (2010). We discuss RX 0152 further in Section 5.

XLSS 0223 contains two galaxies in the core of the cluster that differ by only 0.02 mag. The projected separation of the two galaxies is ∼60 kpc. The brighter of the two, which is selected as the BCG in this study, is considerably more disc-like. In the higher resolution ACS images, the isophotes are distorted, which is perhaps an indication of an ongoing merger.

XMMXCS 2215 contains several galaxies within the core that are almost as bright as one another. The galaxy we selected as the BCG is about 15 arcsec north-west of the cluster centre and is the same galaxy selected in earlier works (Collins et al. 2009; Stott et al. 2010). The choice is not unambiguous, as there are several galaxies in this cluster with a similar magnitude. An observation in a different filter may have resulted in a different choice. XMMLSS 2215 is also interesting for another reason. About 2.3 arcmin south of the cluster there is a galaxy that is even brighter than the galaxy that we have selected as the BCG. It is not selected as the BCG of the cluster as it lands outside r_{200}. It is close to a tight knot of galaxies that currently lack redshifts, so we do not know if this knot of galaxies are associated with the main cluster.

RCS 2345 shares a few similarities to XMMXCS 2215. The cluster is relatively open and there are several cluster members throughout the core and beyond with similar magnitudes. The galaxy that fulfils our definition, as the BCG is about 1 arcmin (500 kpc) to the south of what appears to be the core of the cluster. It is the most isolated BCG in our sample.

We note that modifying our BCG selection criteria by reducing the radius over which BCGs are selected – from r_{200} to r_{500} – and by treating the two clumps of RX 0152 as separate clusters would

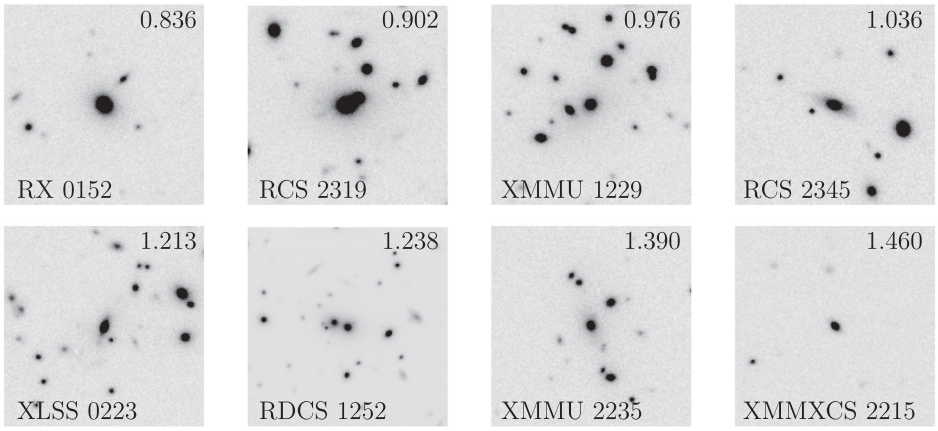

Figure 1. K_s-band image cutouts centred on the HCS BCGs. With the exception of RDCS 1252, the images are 18 arcsec on a side, which corresponds to 140 kpc for the nearest BCG and 155 kpc for the most distant. For RDCS 1252, the image covers twice the area. Annotating each image are the shortened version of the cluster name and the redshift of the cluster. From left to right and from top to bottom, clusters are ordered in redshift. North is up and east is to the left.

Table 4. J- and K_s-band photometry of the BCGs in the HCS clusters.

Name	RA (J2000)[a]	Dec.	Redshift	K_s (mag)	$J-K_s$ (mag)
RCS 231953+0038.0	23:19:53.43	+00:38:13.4	0.9013	16.381 (0.007)	–
RCS 234526−3632.6	23:45:24.94	−36:33:47.9	1.0380	17.411 (0.008)	–
RDCS J1252.9−2927	12:52:54.42	−29:27:17.6	1.2343	17.238 (0.017)	1.888 (0.011)
RX J0152.7−1357	01:52:45.87	−13:56:58.6	0.8342	16.657 (0.010)	–
XLSS J0223.0−0436	02:23:03.72	−04:36:18.2	1.2100	17.616 (0.008)	1.932 (0.009)
XMMU J1229.4+0151	12:29:29.29	+01:51:22.0	0.9740	17.255 (0.015)	–
XMMU J2235.3−2557	22:35:20.85	−25:57:39.8	1.3943	17.317 (0.026)	1.960 (0.019)
XMMXCS J2215.9−1738	22:15:56.20	−17:37:49.9	1.4545	18.650 (0.011)	1.890 (0.016)

[a]Coordinates are those of the BCG.

not affect our sample of BCGs significantly. Apart from gaining an additional BCG from the southern clump in RX 0152, only the BCG in RCS 2345 would change.

It is worth reflecting on how robust our selection is to spectroscopic incompleteness. If the BCG occurs within 250 kpc of the cluster centre and has a $J-K_s$ colour that places it within 0.2 mag of the red sequence, then we will have selected it, as our spectroscopy is 100 per cent complete for objects that are up to three times brighter than the object that was chosen as the BCG. If it lies beyond this radius, then there is a small chance that we would not have selected it. Within 500 kpc of the cluster centres, our spectroscopy for objects that are up to three times as bright as the chosen BCG is 85 per cent complete. As noted earlier, only the BCG of RCS 2345 is significantly more than 250 kpc from the centre of its cluster. It therefore seems unlikely that we have missed many BCGs.

3.2 Photometry

Following Collins et al. (2009), Stott et al. (2010) and Lidman et al. (2012), we use `MAG_AUTO` in SExtractor to estimate the total K_s-band magnitude of the BCG in each cluster and use aperture magnitudes to compute $J-K_s$ colours. The colours are computed within a 16 kpc diameter aperture after first matching the PSFs in the J- and K_s-band images.

The error in `MAG_AUTO` is estimated from the distribution of integrated counts in circularized apertures that are randomly placed in regions where there are no visible objects. The error in the aperture magnitudes, which are used to derive colours, are estimated in the same way. These errors are added in quadrature as an estimate of the error in the colour. Further details on the methods used to compute the magnitudes and colours of the BCGs can be found in Lidman et al. (2012). In Table 4, we list coordinates, redshifts, colours and magnitudes of the BCGs.

In Fig. 2, we plot the K_s-band magnitude of the BCGs in our sample as a function of redshift. In this figure, we also plot the K_s-band magnitude of BCGs from other clusters (Collins et al. 2009; Stott et al. 2010; Lidman et al. 2012). As noted in Lidman et al. (2012), the BCGs in the high-redshift subsample – defined as BCGs with redshifts greater than $z=0.8$ – are systematically fainter than the model that best describes the evolution in the $J-K_s$ colour with redshift. The $J-K_s$ colours of the BCGs are shown in Fig. 3. The model is a composite of two models from Bruzual & Charlot (2003), consisting of a model that has solar metallicity and a model that has a metallically that is two-and-a-half times higher. Both models have an exponentially falling star formation rate with an e-folding time of 0.9 Gyr and a formation redshift of $z=5$. Additional details on the model can be found in Lidman et al. (2012).

Five of the clusters in our sample were also observed in the K_s band by Collins et al. (2009) and Stott et al. (2010) using MOIRCS[9] on the Subaru Telescope. Collins et al. (2009) and Stott et al. (2010) compute magnitudes in exactly the same manner as we do here, so we can compare the fluxes we derive with theirs. We find a mean offset of 0.12 mag with a dispersion of 0.04 mag, indicating a small

[9] MOIRCS stands for Multi-Object InfraRed Camera and Spectrograph.

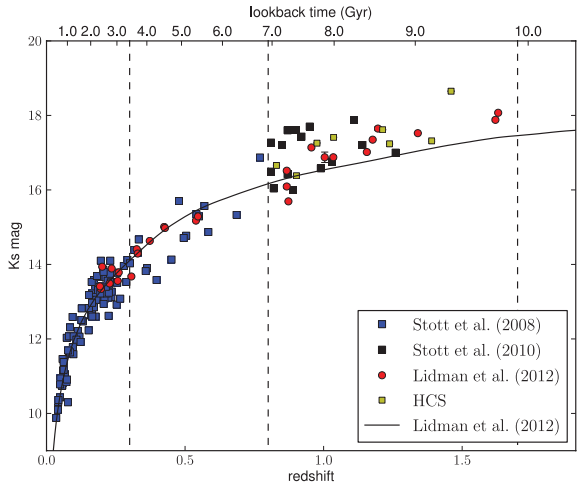

Figure 2. The observer-frame K_s-band magnitude of BCGs as a function of redshift. The data from this paper are plotted as the yellow squares. Red circles beyond $z \sim 0.8$ are BCGs in the SpARCS clusters, while those below $z \sim 0.8$ are BCGs in the CNOC1 clusters. The blue and black points are from Stott et al. (2008) and Stott et al. (2010). The vertical dashed lines divide the sample into three redshift regions, labelled low, intermediate and high. The predicted K_s magnitudes of the best-fitting model used in Lidman et al. (2012) is shown as the black continuous line. The normalization of the model is set so that half of the data in the low-redshift bin lies above the model. Note how the data from this paper land within the region covered by data from earlier works and how most of the points in the high-redshift bin land above the model.

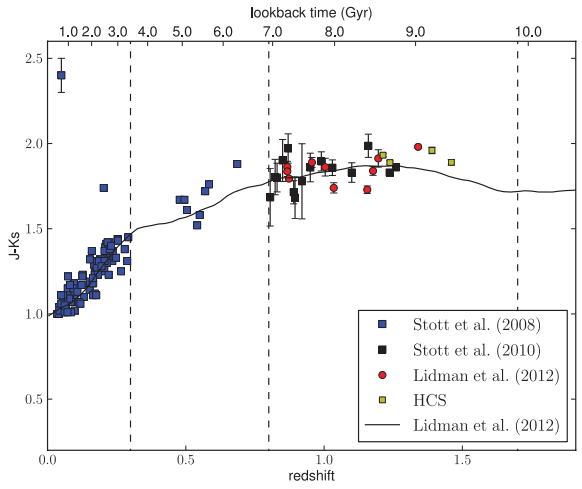

Figure 3. The observer-frame $J - K_s$ colour of BCGs as a function of redshift. The symbols have the same meaning as those in Fig. 2. The blue point in the upper-left corner gives an indication of the uncertainty in the measurements from Stott et al. (2008). Not all BCGs that were observed with HAWK-I have J-band data from HAWK-I, so these BCGs are not shown, The black continuous line represents the model that is used in Lidman et al. (2012) to match the observed colour over the entire redshift range covered by the data. The model adequately describes the average trend in colour from $z \sim 0$ to $z \sim 1.5$. See the text for a description of the model.

difference between the two data sets. On average, the magnitudes reported here are brighter. Offsets in the image zero-points is one possible explanation for the difference. Differences in image quality between the two data sets is another, since image quality affects the size of the aperture that is used in computing `MAG_AUTO`. The K_s-band image quality of the five clusters in common with the sample of clusters in Stott et al. (2010) ranges from 0.31 to 0.38 arcsec, with a mean of 0.34 arcsec. This compares to a mean image quality of ∼0.5 arcsec for clusters in Stott et al. (2010). We degraded the image quality of our data to 0.5 arcsec to see how `MAG_AUTO` for the BCGs changed. On average, the BCGs became 0.05 mag brighter, with considerable scatter between BCGs. The change exacerbates the disagreement in the photometry.

Lidman et al. (2012) used the difference between the model and the observer-frame K_s-band magnitudes to estimate that the stellar mass of BCGs increases by a factor of 1.8 between $z \sim 0.9$ and $z \sim 0.2$. Since all but four of the BCGs in this Fig. 2 are also in Lidman et al. (2012), we do not repeat the analysis here. We do note, however, that the K_s-band magnitude of these BCGs (the BCGs in RCS 2319, RCS 2345, XMMU 1229 and RX 0152) are similar to the K_s-band magnitude of the BCGs at $z \sim 1$.

Instead, we examine the prevalence of close companions to the BCG. Lidman et al. (2012) noted that merging might be the mechanism by which BCGs accrued most of their stellar mass. By examining the prevalence of close companions to BCGs in a large enough sample of clusters, we might be able to see evidence of this.

4 BRIGHT NEARBY COMPANIONS

4.1 The observed number of bright nearby companions

Direct inspection of the K_s-band images reveals that several BCGs have nearby companions that are amongst the brightest galaxies in their respective clusters. Examples include the BCG of RDCS 1252, in which the 2nd BCG is only 15 kpc from the BCG, and SpARCS 1616, in which the 3rd BCG is 22 kpc from the BCG.

To quantify this, we plot in Fig. 4 the number of cluster galaxies – all spectroscopically confirmed – in annuli that are 20 kpc thick, starting from 8 kpc from the BCG and extending out to ∼0.5 Mpc. The lower limit in the first annulus corresponds to the distance at which we can clearly separate galaxies down to the magnitude limit that is probed by the spectroscopy. At the typical redshift of the clusters, this corresponds to about 1 arcsec on the sky. The plot is made for two subsamples: the 2nd, 3rd and 4th brightest cluster members added together to make the first subsample (green bins in Fig. 4), and all galaxies that are between the 10th and 50th brightest cluster members (blue bins).

We have excluded any BCG that is more than 250 kpc from the luminosity-weighted centre of its cluster. The excluded BCGs are the BCGs of SpARCS 1051, SpARCS 1634, RCS 2345 and RX 0152. The distance limit is chosen for a couple of reasons. First, the limit has been used in computing the merger rate at much lower redshifts (Edwards & Patton 2012), so we choose the same threshold to allow a more direct comparison between the merger rates at low and high redshifts. The fraction of excluded BCGs is ∼0.2 and is similar to the fraction excluded in Edwards & Patton (2012), but lower than the fraction of non-central BCGs in Skibba et al. (2011), who define non-central BCGs differently. Secondly, it is possible that some of these far-flung BCGs may not be the direct progenitors of the BCGs that we see at lower redshifts, a point emphasized in De Lucia & Blaizot (2007). There is observational evidence for this in at least one of the clusters. In RX 0152, for example, it is likely that we would have identified a more centrally located galaxy as the BCG if we had observed the cluster a few 100 Myr later. The central region of the northern clump in RX 0152 is dominated by two galaxies that are likely to merge within a few 100 Myr. If they did, the resulting galaxy might become the BCG. We will comment more on this interesting cluster later.

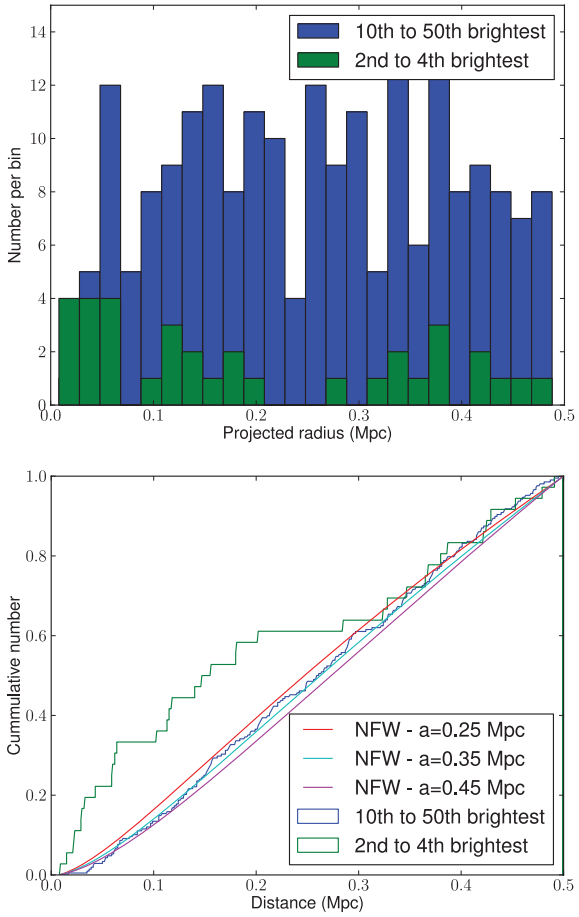

Figure 4. Upper panel: histograms showing the projected radial distance of the 2nd to 4th brightest cluster members (in green) and the 10th to 50th brightest cluster members (in blue) from the BCG. The bin width is 20 kpc. Lower panel: the unbinned cumulative histogram of the two samples together with integrated NFW profiles with three different core radii. Note the difference between the two subsamples.

We note that by changing our selection so that the brightest galaxy in the northern clump of RX 0152 is marked as the BCG, or by including all BCGs outside the 250 kpc distance limit does not alter our conclusions. However, these BCGs are a potential source of bias in other studies. For example, the growth in the stellar mass of BCGs as a function of redshift will be biased low if one includes galaxies that do not become part of the BCG at a later time, even though these galaxies are the brightest in the cluster at the time they were observed.

It is apparent in Fig. 4 that there is a significant excess of galaxies that are classified as the 2nd, 3rd and 4th brightest galaxies of the cluster in the inner three annuli (i.e. out to ∼70 kpc) compared to the annuli that are further out. The excess is still visible if we consider just the 2nd brightest galaxy, the 2nd and 3rd brightest galaxies, or the 2nd, 3rd, 4th and 5th brightest galaxies added together. We will return to these bright galaxies after examining the distribution of fainter galaxies.

In contrast to the brightest galaxies, the number of galaxies that are fainter than the 10th brightest galaxy but brighter than the 50th is much less concentrated. The inner most bin for this subsample has only one object. Not all clusters have 50 spectroscopically confirmed members. For these clusters we include all galaxies that are fainter than the 10th brightest member.

A two-sided KS test reveals that the probability (or *P*-value) that the two samples are drawn from the same distribution is 1 per cent. This low value provides support for rejecting the null hypothesis, i.e. the two samples are drawn from the same distribution. However, the *P*-values are sensitive to the clusters used and to the radius out to which the distributions are measured. For example, limiting the radius over which the histograms are compared to 300 kpc results in a *P*-value of 0.1 per cent. On the other hand, restricting the faintest members in the second sample to progressively brighter galaxies results in higher *P*-values. For these reasons, we take results of the KS test as very suggestive rather than conclusive. The difference between the two distributions may become clearer once a larger sample of clusters becomes available.

The results of the KS test may be affected by differences in how the spectroscopic completeness of the two subsamples changes with projected radius. The success of obtaining a spectroscopic redshift depends on several factors, so the radial dependence of the spectroscopic completeness may be different for bright and faint objects. To examine this issue, we compare curves that are obtained by integrating projected Navarro–Frenk–White (NFW) profiles (Bartelmann 1996; Navarro, Frenk & White 1996) with a range of core radii, a, to the cumulative histograms of the two subsamples. The comparison is made in the lower plot of Fig. 4. For the clusters in our sample, these core radii correspond to concentrations ($c_{200} = r_{200}/a$) ranging from 2.2 to 4, which covers the range expected for massive clusters at $z \sim 1$ (Duffy et al. 2008).

The radial distribution of the fainter cluster galaxies is consistent with an NFW profile that has a core radius of 0.35 Mpc. A KS test results in a *P*-value that is close to 1. There is no strong evidence for a radial dependence in the spectroscopic incompleteness in this subsample. The subsample containing the brighter galaxies has a radial distribution that is considerably different to that of the NFW profiles shown in Fig. 4. This could be interpreted as incompleteness in the bright galaxy subsample at large radii. However, we consider this explanation to be unlikely. Out to 250 kpc, we estimate that the spectroscopic completeness is 85 per cent for objects that are brighter than 25 per cent of the Ks-band luminosity of the BCG. Out to 500 kpc, this only drops to 78 per cent.

Instead, we believe that most of the difference between the two subsamples is real and that the difference has a physical explanation. A plausible physical explanation for the difference between the bright and faint samples is dynamical friction. Dynamical friction is more effective in bringing large galaxies and galaxy groups into the core region than it is in bringing in small galaxies. The radial segregation between bright and faint clusters galaxies is observed in nearby massive groups and clusters (Pracy et al. 2005; Zandivarez & Martínez 2011). However, see Mei et al. (2007) for a different result in the Virgo cluster.

We now return our attention to the bright galaxies shown in Fig. 4. The excess of galaxies in the innermost annuli implies that the transverse velocities of most of these galaxies are unlikely to be very high. If they were high, say comparable to the velocity dispersion of the cluster, then the excess in the inner most annuli would be erased. We note that the circular speed of the NFW profile in this central region is about half that at the core radius. If we make the additional assumption that clusters are roughly spherical (an assumption that we will return to later), then the excess also implies that most of these galaxies are not strongly projected along the line of sight to the BCG.

The inner most annulus contains four galaxies. The coordinates of these galaxies, their K_s-band flux relative to the BCG in their

Table 5. Bright cluster members that have a projected distance that is between 8 and 28 kpc of the BCG.

Name	RA (J2000)[a]	Dec. (J2000)[a]	Separation (kpc)	Flux ratio	Rank	Relative velocity (km s^{-1})[b]
RCS 231953+0038.0	23 19 53.36	+00 38 14.1	9.66	0.327	4	363
RDCS J1252.9−2927	12 52 54.55	−29 27 17.1	14.93	0.805	2	470
XMMU J2235.3−2557	22 35 20.72	−25 57 37.7	23.20	0.464	3	1415
SpARCS J161641+554513	16 16 41.63	+55 45 12.9	22.26	0.841	3	167

[a]Coordinates are those of the companion.
[b]The relative velocity is the line-of-sight velocity difference between the companion and its BCG. For the HCS clusters, the uncertainty is around 100 km s^{-1}. For the SpARCS clusters, it is double this.

cluster, their ranking in terms of brightness, and their line-of-sight velocities with respect to their BCGs are shown in Table 5. Their proximity to the BCG means that these galaxies could potentially merge with their respective BCGs in less than 1 Gyr (Lotz et al. 2011). There are no other galaxies that are within a factor of 4 in mass with respect to the BCG (i.e. a potential major merger) and this close to the BCG.

4.2 The expected number of bright nearby companions

Given the time-scale for how long it takes a bright nearby companion to merge with the BCG, one can estimate the number of close companions one should see if major mergers are the principal mechanism for the growth in the stellar mass of BCGs. Since the time-scales are only approximately known, we examine a range of time-scales. At the lower end is the time it takes for two galaxies to merge once they are already in the process of merging. This is of the order of a few crossing times (Binney & Tremaine 2008). At a distance of 30 kpc, the crossing time for a BCG with a velocity dispersion of 250 km s^{-1} is around 70 Myr, resulting in a merging time-scale of around 200 Myr. It is over this sort of time-scale that one would expect to see direct evidence of the merger occurring, i.e. evidence of diffuse tidal tails, highly distorted isophotes and broad fans.

When direct evidence for merging is not apparent, the time-scale will be larger. Lotz et al. (2011) derive a merger time-scale of 600 Myr for pairs of field galaxies that have a projected separation that ranges between 7 and 21 kpc, a velocity difference that is less than 500 km s^{-1} and a mass ratio that is in the major merger mass range.

Kitzbichler & White (2008) provide a formula to compute the time-scale for merging for galaxies that have a line-of-sight velocity difference that is less than of 300 km s^{-1}. For a pair of galaxies at $z \sim 1$ with a projected distance of 21 kpc and a combined stellar mass of 5×10^{11} M$_\odot$, the time-scale is 500 Myr, which is similar to the time-scale found by Lotz et al. (2011).

The time-scales derived by Lotz et al. (2011) and Kitzbichler & White (2008) apply equally well to galaxy pairs in the centre of clusters (we return to this point in Section 5.2). By Newton's first theorem, mass outside the orbit of the galaxy pair is not felt. For our work, the time-scales of Lotz et al. (2011) and Kitzbichler & White (2008) are the most appropriate ones to use. However, we also examine what happens if the time-scale is considerably longer, i.e. 1.0 Gyr.

In Fig. 5, we plot the number of major mergers one would expect to see in our sample of 14 high-redshift clusters as a function of how much the BCG grows between redshift $z = 0.9$ and $z = 0.2$. We make the assumption that the major merger rate is constant with redshift. We compute the number for three time-scales, 200, 600 and 1 Gyr.

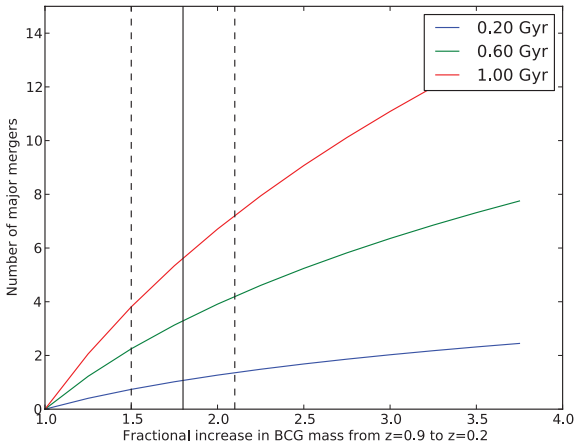

Figure 5. The number of major mergers one would expect to see in our sample of 14 high-redshift clusters as a function of how much the BCG grows between redshift $z = 0.9$ and $z = 0.2$. The number is plotted for three merger time-scales: 0.2, 0.6 and 1.0 Gyr. The vertical solid line represents the growth that has been measured by observations and the dashed line is the uncertainty (Lidman et al. 2012). For a time-scale of 0.6 Gyr, we would expect that three major mergers would occur in our 14 high-redshift clusters within 600 Myr. This is remarkably close to what we observe.

The vertical line represents the growth that has been measured by observations (Lidman et al. 2012). In this plot, we have assumed that all the mass growth is due to mergers with galaxies that are 62.5 per cent of the mass of the BCG,[10] and that 50 per cent of the companion is accreted on to the BCG. High-resolution simulations suggest that between 50 and 80 per cent of the mass of mergers will be distributed throughout the cluster (Conroy, Wechsler & Kravtsov 2007; Puchwein et al. 2010) and visible as intracluster light. If only 20 per cent of the mass of the companion is accreted on to the BCG, these curves move up by a factor of 2.5.

The vertical line intersects the middle green curve in Fig. 5, which represents a merging time-scale of 600 Myr, at ∼3. In other words, one would expect to see evidence for three major mergers in the 14 distant clusters of our sample. Interestingly, there are three galaxies in Table 5 that we identify as galaxies that will merge with the BCG within 600 Myr: one of each in RDCS 1252, SpARCS 1616 and RCS 2319. The galaxy in XMMU 2235 is moving too fast with respect to the BCG to merge with the BCG over this time-scale.

We can use Fig. 5 to estimate the number of major mergers that are expected to occur within the next 200 Myr. This is the time-scale over which one should see evidence of an interaction through,

[10] This is simply the average mass of the companion in a 1:1 merger and the companion in a 1:4 merger.

for example, diffuse fans, distorted isophotes and tidal tails. Using Fig. 5, we find that we should see one such case in our sample of 14 clusters. Interestingly, there is one pair where there is evidence of an ongoing interaction. This is the pair in RDCS 1252 (Blakeslee et al. 2003; Rettura et al. 2006).

5 DISCUSSION

5.1 Sources of uncertainty

There is, of course, considerable uncertainty in the estimated number of major mergers. First and foremost, there is the uncertainty that comes from small number statistics. Out of 14 clusters that were examined, we find that there are three galaxies that are likely to result in a major merger with the BCG within 600 Myr. We use the beta distribution to compute confidence intervals (Cameron 2011) on the probability that a cluster contains a galaxy pair of this type at any one time. The 68.3 per cent confidence interval goes from 0.14 to 0.36. This is a very broad range.

There is also the possibility that some of the galaxies that we have assumed to be near to the BCG are in fact projections along the line of sight. The probability of this increases if clusters are extended along the line of sight. All of our clusters are selected either as overdensities in red sequence galaxies (e.g. the clusters from SpARCS and RCS) or as extended X-ray sources (e.g. RDCS 1252). Both types of selection preferentially select clusters that are extended along the line of sight.

The cluster RDCS 1252 is an interesting case. By analysing the angular structure of cluster members together with their velocities, Demarco et al. (2007) conclude that RDCS 1252 consists of two subclusters in the process of merging, with the BCG of the cluster centred in one of the subclusters and the 2nd brightest galaxy centred in the other. RDCS 1252 provides support for the idea that some clusters are extended along the line of sight. In such cases, the two brightest galaxies in the cluster may be much further apart than we expected.

Nevertheless, the central pair of galaxies in RDCS 1252 provide us with more information. Blakeslee et al. (2003) and Rettura et al. (2006) both find evidence of an S-shaped residual linking the centre of the two brightest galaxies in the model-subtracted images, thus providing a clear sign that the galaxies are merging and are indeed near to each other.

5.2 Velocity offsets

In computing the merger time-scale for the BCG and its companion, we have argued that we can use the time-scales that have been computed for field galaxies. This is only valid if the BCG and its companion are centred in the cluster and at rest with respect to it. If these conditions are not met, then the BCG and its companion would be subject to tidal forces from the cluster. This would increase the merger time-scale and perhaps even prevent the BCG and its companion from merging (Mihos 2003).

We examine the spatial and dynamical properties of the three BCGs – the BCGs in SpARCS 16116, RDCS 1252 and RCS 2319 – that we have identified as undergoing a potential major merger within ∼500 Myr. All three are spatially well centred in their respective clusters. Dynamically speaking, we can only compare the redshift of the BCG with respect to median redshift of the cluster galaxies, which we will use as a proxy for the cluster redshift. As can be seen in Table 6, within errors, the velocity offsets of the BCGs in SpARCS 1616 and RCS 2319 are consistent with zero, meaning that the BCGs are practically at rest with respect to the cluster. Using the merger time-scale that has been used for field studies is therefore reasonable.

Table 6. Velocity offset between the cluster redshift and the BCG.

Short name	Velocity offset (km s^{-1})
RX J0152.7−1357	290 ± 240
RCS 231953+0038.0	170 ± 190
XMMU J1229.4+0151	230 ± 210
RCS 234526−3632.6	−290 ± 160
XLSS J0223.0−0436	430 ± 200
RDCS J1252.9−2927	500 ± 160
XMMU J2235.3−2557	−540 ± 210
XMMXCS J2215.9−1738	670 ± 170
SpARCS J003442−430752	−140 ± 220
SpARCS J003645−441050	300 ± 230
SpARCS J161314+564930	−180 ± 230
SpARCS J104737+574137	80 ± 220
SpARCS J021524−034331	−60 ± 180
SpARCS J105111+581803	−40 ± 190
SpARCS J161641+554513	−30 ± 190
SpARCS J163435+402151	30 ± 190
SpARCS J163852+403843	−100 ± 190
SpARCS J003550−431224	1030 ± 240

The BCG of RDCS 1252, however, is not at rest with respect to its cluster. As noted in the previous section, RDCS 1252 appears to consist of two merging subclusters (Demarco et al. 2007), with the BCG centred in one subcluster and its companion centred in the other. It seems likely that cluster tides will play an important role in setting the time-scale over which these two galaxies will merge. There seems little doubt that they will merge, as there is evidence of an interaction between the BCG and the 2nd brightest galaxy in this cluster (Blakeslee et al. 2003; Rettura et al. 2006).

Looking at the entire sample, we see that a few other BCGs are not at rest within their respective clusters. The most notable of these is the BCG in SpARCS 0035. Such offsets are indicative of a cluster merger. SpARCS 0035 is discussed further in Rettura et al. (in preparation).

5.3 RX 0152

In Section 4, we excluded four clusters because the BCG was more than 250 kpc from the luminosity-weighted centres of the clusters. One of the excluded clusters was RX 0152.

As noted earlier, RX 0152 consists of at least three dynamically distinct clumps (Demarco et al. 2005, 2010b). The BCG is not centred in any of the clumps: instead, it is centred about 35 arcsec (270 kpc) north-east of the northern clump. Closer inspection of the galaxies that are centred in the two biggest clumps reveals that both have bright, nearby companions, as illustrated in Fig. 6.

Both galaxies in the northern clump are cluster members. They are separated by 12 kpc and differ in velocity by 280 km s^{-1}. They almost have the same brightness, differing in K_s-band flux by only 1 per cent. Using the arguments presented in Section 4, it is likely that these galaxies will merge within a few 100 Myr. If these galaxies do merge and if all of the mass stays in the descendent of the merger, then the descendent will become the brightest galaxy in the cluster. Intriguingly, in the deep HAWK-I data, there appears to be material possibly extending from this pair to the north-east. The material is

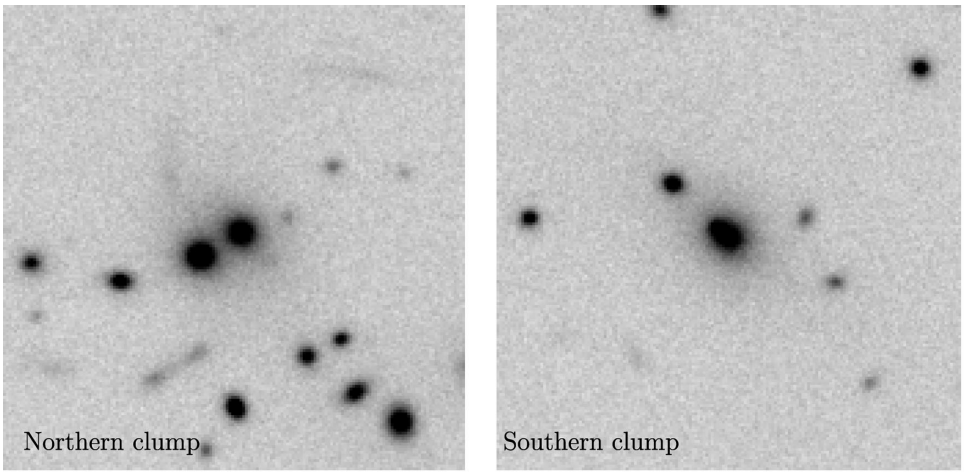

Figure 6. HAWK-I K_s-band images of the central galaxies in the two largest clumps of RX 0152 (Demarco et al. 2005). Left: the central region of the northern clump. Note the faint, gently curving material towards the north-east of the pair. In the higher resolution ACS images, it seems to be a smaller galaxy that is interacting with the two brighter galaxies. Alternatively, it could be a strongly lensed background galaxy. Right: the central region of the southern clump. Note the very close companion to the central galaxy of the southern clump, which can be seen as an extension of the isophotes to the north-east of the galaxy. Nantais et al. (2013) have noted that this object is very compact in the ACS images, which is an indication that it is an advanced state of merging with the bigger galaxy. The images are 18 arcsec on a side, which corresponds to 140 kpc at the redshift of the cluster. North is up and east is to the left.

also visible in the ACS image. It may be a background arc, although the orientation is more radial than tangential, or it could be material from a third galaxy that is in the process of being destroyed by its two much more massive companions.

The central region in the southern clump is actually a triplet of galaxies, consisting of a pair of cluster members that are 20 kpc apart and a 3rd galaxy that is only 3.5 kpc from the brightest galaxy in the triplet, which was the galaxy chosen as the BCG in Stott et al. (2010). Unfortunately, we do not have a redshift for the 3rd galaxy. However, as noted in Nantais et al. (2013), the third galaxy in the ACS images appears to be very compact when compared to cluster galaxies of similar brightness. This is indicative of an ongoing merger. The halo of the galaxy has been stripped by its brighter neighbour. The redshifts of the other two galaxies are, within the errors, identical, which means that the relative velocity of the galaxies differ by less than 100 km s^{-1}. These two galaxies could also merge within a few 100 Myr. If all three galaxies were to merge and if there was no subsequent star formation, then the brightness of the resulting galaxy would be comparable to the brightness of what is now the BCG.

5.4 Comparison with low-redshift subsamples

A number of studies have estimated the number of bright galaxies that are close to BCGs in nearby galaxy clusters. Liu et al. (2009) estimated that about 49 BCGs out of a sample of 515 BCGs in the redshift interval $0.03 \leq z \leq 0.12$ have a companion that is (i) within a projected distance of 7–30 kpc of the BCG and (ii) within 2 mag of the SDSS r-band magnitude of the BCG. They apply a further restriction, which applies to both the BCG and its companion. The $g - r$ colour of both galaxies must be greater than 0.7.

The criteria adopted by Liu et al. (2009) are broadly similar to the ones used in this paper. They find that 1 BCG in 10 have a bright nearby companion, whereas we find that 3 BCGs in 14 have a nearby bright companion. The number of companions in our more distant clusters is higher; however, given the small number of clusters in the high-redshift sample, it is premature to cite this as strong evidence that the number of bright nearby companions to BCGs in distant clusters is increasing with redshift. We return to this point in the following section.

Liu et al. (2009) then go on to examine the number of BCGs that show direct evidence of merging with their nearby companion. Evidence of a merger includes tidal tails, distorted isophotes and broad fans. Out of 49 close pairs, 18 or one-third show evidence for a merger taking place. While we again stress that the number of BCGs in our high-redshift sample is small, one of our three pairs, the pair in RDCS 1252, shows evidence for a merger.

Liu et al. (2009) estimate that BCGs are increasing their stellar mass at a rate of 2.5 per cent $(t_{\rm merger}/0.3\,{\rm Gyr})^{-1}(f_{\rm mass}/0.5)$, where $t_{\rm merger}$ is the time-scale for the merger to take place and $f_{\rm mass}$ is the fraction of companion's stellar mass that is accreted on to the BCG. In a separate study, Edwards & Patton (2012) find that BCGs at $z \sim 0.3$ are adding as much as 10 per cent of their stellar mass through mergers, both minor and major, over 0.5 Gyr, which is considerably higher than the rate in Liu et al. (2009). However, recall that Liu et al. (2009) only include cases where there is direct evidence of a merger and only major mergers. The two results differ because of the broader definition of potential mergers and the broader mass range used in Edwards & Patton (2012). They also probe different redshifts.

In our study of 14 high redshift clusters, we find that BCGs are accreting mass at a rate of 7 per cent $(t_{\rm merger}/0.6\,{\rm Gyr})^{-1}$. This estimate assumes that half of the mass of the companion is accreted on to the BCG and half is distributed more broadly throughout the cluster. Our rate is higher than that inferred by Liu et al. (2009). On the other hand, it is lower than the rate computed for low-redshift clusters in Edwards & Patton (2012); however, we do not include minor mergers, whereas Edwards & Patton (2012) do, so part of the difference is in part due to the broader mass range used in Edwards & Patton (2012).

While our sample is too small to test for a change in the major merger rate with redshift, it is clear that major mergers are occurring

at $z \sim 1$ and that the rate is comparable to the rate at lower redshifts. If major mergers contribute as much mass as minor mergers, and *N*-body simulations suggest that they contribute more (Hopkins et al. 2010; Laporte et al. 2013), then major mergers are not only an important mechanism for the build up of stellar at $z \sim 1$, they are an important mechanism between $z \sim 1$ and today.

Theoretically, one would expect major mergers to be more common at higher redshifts. The accretion rate for massive clusters peaks between $z = 1.5$ and $z = 2$ (Fakhouri, Ma & Boylan-Kolchin 2010), and as clusters get larger, the dynamical friction time-scale for galaxies of a given mass increases, so it takes longer for a galaxy to sink into the core. For these reasons, one would expect BCGs to experience fewer major mergers at lower redshifts. We now compare our results with the results from models.

5.5 Comparison with models

Hopkins et al. (2010) use semi-empirical models to estimate the major merger[11] rate as a function of stellar mass and redshift. At $z \sim 1$, they find that the major merger rate per galaxy varies between $\sim$0.15 and $\sim$0.4 Gyr^{-1} for galaxies with stellar masses between 10^{11} and 10^{12} M$_\odot$. The merger rate increases quickly with stellar mass and with redshift.

This mass range covers the range of stellar masses of the BCGs in our sample, which varies between 10^{11} and 8×10^{11} M$_\odot$, with a median mass of $\sim 3 \times 10^{11}$ M$_\odot$. Our BCGs vary in redshift from $z = 0.84$ to $z = 1.46$, with a median of $z \sim 1.1$.

If we use the more restrictive definition of what constitutes a major merger used in Hopkins et al. (2010), we find that 2 out of 14 of the BCGs in our sample – the 3rd galaxy has a mass ratio 0.327, and therefore just fails to meet the more restrictive definition – are likely to experience a major merger within 600 Myr. This translates to a rate of 0.25 major mergers per Gyr, which is fully consistent with the rates derived in Hopkins et al. (2010). Using the broader definition that we have used throughout the paper, we find a rate of 0.4 major mergers per Gyr.

As noted in Section 5.4, we find a higher fraction of bright nearby companions in our sample than others have found in samples at lower redshifts. We find them to be about a factor of about 2 more common. Over the stellar mass range covered by the BCGs in our sample, Hopkins et al. (2010) find that the major merger rate increases between $z = 0$ and $z = 1$ by a factor that varies between 2 and 4. This is consistent to what we infer from observations.

While there is consistency between models and observations, one needs to be mindful of potential biases that come from the way clusters are selected at low and high redshifts. The clusters in our sample are some of the most massive clusters that we know of at these high redshifts. By today, they would have increased in mass significantly, from a median mass of 3.6×10^{14} M$_\odot$ at $\sim$1.1 to a median mass of 1.3×10^{15} M$_\odot$. By today, the average cluster in our sample of high-redshift clusters would be more massive than the average cluster in the sample used in, for example, Liu et al. (2009). Since the properties of the BCG correlates with the properties of the cluster in which it lives (e.g. more massive clusters have more massive BCGs), it is not unreasonable to expect that the major merger rate does too. Comparing this rate in cluster samples that span different mass ranges may lead to a biased view of how this rate changes with redshift. Currently our samples are too small to explore how significant this bias may be.

[11] Note that Hopkins et al. (2010) use a more restrictive range of mass ratios than we do here. They define a major merger as one in which $\mu_\star$ lies within the range $0.33 < \mu_\star < 1$.

6 SUMMARY AND FUTURE WORK

We combine 10 distant clusters from SpARCS with the 9 clusters of the HCS to build a sample of 19 galaxy clusters between $z = 0.84$ and $z = 1.46$. Our sample contains over 600 spectroscopically confirmed cluster members. We use this sample to examine the frequency of bright cluster members that are likely to merge with the BCG within 600 Myr.

After excluding one cluster because of the uncertainty in identifying the BCG – due to the chance projection of a much nearer face-on spiral galaxy close to the cluster core – and four others because the BCGs are located more than 250 kpc from the cluster centres, we find that 3 of the 14 BCGs are likely to experience a major merger within 600 Myr. While the statistical uncertainty stemming from the small number of clusters in our sample is large, the number of mergers is similar to the number of mergers that are predicted by theory and to the number that would be needed to build the stellar mass of BCGs by a factor of $\sim$2 between redshift $z = 0.9$ and $z = 0.2$, under the assumptions that major mergers contribute most of the accreted stellar mass and that half of the mass of the companion is accreted on to the BCG. The factor of 2 increase in the stellar mass between redshift $z = 0.9$ and $z = 0.2$ has been measured from observations (Lidman et al. 2012) and predicted by *N*-body models (Laporte et al. 2013).

The data are consistent with the notion that the majority of the stellar mass that is accreted on to BCGs between $z \sim 1$ and today comes from major mergers. However, they do not exclude the possibility that minor mergers could play an important role in shaping how BCGs appear today. In future work (Rettura et al. in preparation), we will examine the size of the BCGs in our sample and compare them to BCGs at lower redshifts. It is expected that major mergers increase the size of the galaxy linearly with the amount of mass accreted, whereas minor mergers are expected to increase the size of the galaxy more quickly than this.

ACKNOWLEDGEMENTS

The authors thank Chris Collins, John Stott, Adam Duffy and Darren Croton for useful discussions, and Adam Stanford for making available the redshifts for XMMXCS 2215. The data in this paper were based in part on observations obtained at the ESO Paranal Observatory (ESO programmes 060.A-9284(H) and 084.A-0214). CL is the recipient of an Australian Research Council Future Fellowship (programme number FT0992259). LFB was supported by Fondo National de Desarollo Cientifico y Tecnologico (FONDECYT) grants No. 1085286 and 1120676. WJC is the recipient of an Australian Research Council Professorial Fellowship (programme number DP0877642). JN acknowledges the support provided from FONDECYT research grant number 3120233. RD acknowledges the support provided from FONDECYT research grant number 1100540. GW gratefully acknowledges support from National Science Foundation grant AST-0909198.

REFERENCES

Andreon S. et al., 2005, MNRAS, 359, 1250
Bartelmann M., 1996, A&A, 313, 697
Bildfell C. et al., 2013, MNRAS, 425, 204

Binney J., Tremaine S., 2008, in Spergel D. N., ed., Galactic Dynamics, 2nd edn. Princeton Univ. Press, Princeton, NJ
Blakeslee J. P. et al., 2003, ApJ, 596, L143
Blakeslee J. P. et al., 2006, ApJ, 644, 30
Boehringer H., Mullis C., Rosati P., Lamer G., Fassbender R., Schwope A., Schuecker P., 2005, Msngr, 120, 33
Bremer M. N. et al., 2006, MNRAS, 371, 1427
Brough S., Collins C. A., Burke D. J., Mann R. G., Lynam P. D., 2002, MNRAS, 329, L53
Brough S., Couch W. J., Collins C. A., Jarrett T., Burke D. J., Mann R. G., 2008, MNRAS, 385, L103
Brough S., Tran K.-V., Sharp R. G., von der Linden A., Couch W. J., 2011, MNRAS, 414, L80
Bruzual G., Charlot S., 2003, MNRAS, 344, 1000
Burke D. J., Collins C. A., Mann R. G., 2000, ApJ, 532, L105
Cameron E., 2011, PASA, 28, 128
Casali M. et al., 2006, Proc. SPIE, 6269, 29
Collins C. A. et al., 2009, Nat, 458, 603
Conroy C., Wechsler R. H., Kravtsov A. V., 2007, ApJ, 668, 826
Dawson K. S. et al., 2009, AJ, 138, 1271
De Lucia G., Blaizot J., 2007, MNRAS, 375, 2
Demarco R. et al., 2005, A&A, 432, 381
Demarco R. et al., 2007, ApJ, 663, 164
Demarco R. et al., 2010a, ApJ, 711, 1185
Demarco R. et al., 2010b, ApJ, 725, 1252
Duffy A. R., Schaye J., Kay S. T., Dalla Vecchia C., 2008, MNRAS, 390, L64
Edge A. C., 1991, MNRAS, 250, 103
Edwards L. O. V., Patton D. R., 2012, MNRAS, 425, 287
Eisenhardt P. R. M. et al., 2008, ApJ, 684, 905
Fakhouri O., Ma C.-P., Boylan-Kolchin M., 2010, MNRAS, 406, 2267
Gilbank D. G., Yee H. K. C., Ellingson E., Hicks A. K., Gladders M. D., Barrientos L. F., Keeney B., 2008, ApJ, 677, L89
Gladders M. D., Yee H. K. C., 2005, ApJS, 157, 1
Hopkins P. F. et al., 2010, ApJ, 715, 202
Kitzbichler M. G., White S. D. M., 2008, MNRAS, 391, 1489
Laporte C. F. P., White S. D. M., Naab T., Gao L., 2013, preprint (arXiv:1301.5319)
Lidman C., Rosati P., Demarco R., Nonino M., Mainieri V., Stanford S. A., Toft S., 2004, A&A, 416, 829
Lidman C. et al., 2008, A&A, 489, 981
Lidman C. et al., 2012, MNRAS, 420, 1946
Liu F. S., Mao S., Deng Z. G., Xia X. Y., Wen Z. L., 2009, MNRAS, 396, 2003
Lotz J. M., Jonsson P., Cox T. J., Croton D., Primack J. R., Somerville R. S., Stewart K., 2011, ApJ, 742, 103
McIntosh D. H., Guo Y., Hertzberg J., Katz N., Mo H. J., van den Bosch F. C., Yang X., 2008, MNRAS, 388, 1537
Mei S. et al., 2007, ApJ, 655, 144
Mihos J. C., 2003, in Mulchaey J. S., Dressler A., Oemler A., eds, Carnegie Observatories Astrophysics Series, Vol. 3: Clusters of Galaxies: Probes of Cosmological Structure and Galaxy Evolution. Cambridge Univ. Press, Cambridge
Morokuma T. et al., 2010, PASJ, 62, 19
Mullis C. R., Rosati P., Lamer G., Böhringer H., Schwope A., Schuecker P., Fassbender R., 2005, ApJ, 623, L85
Munoz R., 2009, PhD thesis, Univ Católica de Chile
Muzzin A. et al., 2009, ApJ, 698, 1934
Muzzin A. et al., 2012, ApJ, 746, 188
Muzzin A., Wilson G., Demarco R., Lidman C., Nantais J., Hoekstra H., Yee H. K. C., Rettura A., 2013, ApJ, 767, 39
Nantais J., Flores H., Demarco R., Lidman C., Rosati P., Jee J., 2013, preprint (arXiv:1305.0826)
Navarro J. F., Frenk C. S., White S. D. M., 1996, ApJ, 462, 563
Persson S. E., Murphy D. C., Krzeminski W., Roth M., Rieke M. J., 1998, AJ, 116, 2475
Pirard J.-F. et al., 2004, Proc. SPIE, 5492, 1763
Postman M., Lubin L. M., Gunn J. E., Oke J. B., Hoessel J. G., Schneider D. P., Christensen J. A., 1996, AJ, 111, 615
Pracy M. B., Driver S. P., De Propris R., Couch W. J., Nulsen P. E. J., 2005, MNRAS, 364, 1147
Puchwein E., Springel V., Sijacki D., Dolag K., 2010, MNRAS, 406, 936
Rasmussen J., Mulchaey J. S., Bai L., Ponman T. J., Raychaudhury S., Dariush A., 2010, ApJ, 717, 958
Rettura A. et al., 2006, A&A, 458, 717
Rosati P., Stanford S. A., Eisenhardt P. R., Elston R., Spinrad H., Stern D., Dey A., 1999, AJ, 118, 76
Rosati P. et al., 2004, AJ, 127, 230
Sahlén M. et al., 2009, MNRAS, 397, 577
Santos J. S. et al., 2009, A&A, 501, 49
Skibba R. A., van den Bosch F. C., Yang X., More S., Mo H., Fontanot F., 2011, MNRAS, 410, 417
Skrutskie M. F. et al., 2006, AJ, 131, 1163
Stanford S. A. et al., 2006, ApJ, 646, L13
Stott J. P., Edge A. C., Smith G. P., Swinbank A. M., Ebeling H., 2008, MNRAS, 384, 1502
Stott J. P. et al., 2010, ApJ, 718, 23
Suzuki N. et al., 2012, ApJ, 746, 85
van der Berg R. F. J. et al., 2013, preprint (arXiv:1304.5525)
Whiley I. M. et al., 2008, MNRAS, 387, 1253
Wilson G. et al., 2009, ApJ, 698, 1943
Yee H. K. C., Gladders M. D., Gilbank D. G., Majumdar S., Hoekstra H., Ellingson E., 2007, in Metcalfe N., Shanks, T., eds, ASP Conf. Ser. Vol. 379, Cosmic Frontiers. Astron. Soc. Pac., San Francisco, p. 103
Zandivarez A., Martínez H. J., 2011, MNRAS, 415, 2553

This paper has been typeset from a TEX/LATEX file prepared by the author.